ELSEVIER

Journal of Wind Engineering
and Industrial Aerodynamics 59 (1996) 131–157

JOURNAL OF
wind engineering
AND
industrial
aerodynamics

Damping in structures: its evaluation and treatment of uncertainty

A. Kareem*,[1], K. Gurley[2]

Department of Civil Engineering and Geological Science, University of Notre Dame, 163 Fitzpatrick, Notre Dame, IN 46556, USA

Abstract

This paper concerns the damping in structures with emphasis on treatment of inherent uncertainty in its prediction and estimation. Material or structural damping is addressed as well as damping due to the aerodynamic and hydrodynamic forces of the fluid surrounding the structure. The reported data base on damping information is examined in light of wind sensitive structures that rely heavily on damping for their performance under winds. The basic techniques for estimation of damping from response time histories are reviewed, and the random decrement technique is considered in some detail. The implications of the uncertainty of damping on system response are analyzed in terms of a perturbation technique, second-moment analysis and Monte Carlo simulation. Several simple illustrative examples are provided throughout the text.

Keywords: Aerodynamic damping; Higher mode damping; Hydrodynamic damping; Monte Carlo simulation; Offshore platform; Perturbation technique; Random decrement technique; Second-moment analysis; Structural damping; Uncertainty analysis

1. Background

Estimation of damping in structural systems poses a most difficult problem in structural dynamics. Unlike the mass and stiffness characteristics of a structural system, damping does not relate to a unique physical phenomenon. Damping is often required and it is difficult to engineer it unless external damping systems are introduced in the structural system. The importance of damping is becoming increasingly

*Corresponding author.
[1] Professor.
[2] Graduate student.

PII S0167-6105(96)00004-9

significant as buildings are becoming taller and relatively more flexible. Modern high-rise buildings designed to satisfy lateral drift requirements still may oscillate excessively during wind storms. The level of these oscillations may not be significant enough to cause structural damage but may cause discomfort to the building occupants. The estimates of damping in structural systems have intrinsic variability which makes the assessment of the serviceability limit states more uncertain. Any accurate information concerning the damping values, at the design stage, may certainly alleviate a major source of uncertainty routinely experienced by designers of wind sensitive structures.

Structural damping is a measure of energy dissipation in a vibrating structure that results in bringing it to a quiescent state. The damping capacity is defined as the ratio of the energy dissipated in one cycle of oscillation to the maximum amount of energy accumulated in the structure in that cycle. There are as many damping mechanisms as there are modes of converting mechanical energy into heat. The most important among these are material damping and interfacial damping (Nashif et al., 1984).

The material damping contribution comes from a complex molecular interaction within the material, thus the damping is dependent on the type of material, methods of manufacturing and final finishing processes. The complexity of the situation is further enhanced by the simple reality that material properties often differ from sample to sample, resulting possibly in significant differences in energy losses among distinct members of a structural system. The equations of motion in structural dynamics usually describe a macroscopic behavior, while material damping processes arise from microscopic phenomena. This conflict in the scales leads to a search for phenomenological theories for the representation of structural damping.

The interfacial damping mechanism is Coulomb friction between members and connections of a structural system, and between structural components like partitions and exterior facade. Welded connections tend to reduce the contribution of interfacial damping as compared to the bolted connections. Soil–structure interaction also contributes towards the overall damping depending on the soil characteristics (e.g., Novak, 1974; Wolf, 1988).

Aerodynamic or hydrodynamic damping is experienced by a structure vibrating in air or water. In cases of ocean structures, both damping sources may contribute simultaneously. Generally, the aerodynamic damping is quite small compared to mechanical damping of the structure and it is positive in low to moderate reduced wind speeds (speed normalized by frequency and body width), but at certain wind speeds negative aerodynamic damping may be experienced. The hydrodynamic damping is relatively large, especially for ocean structures in the presence of waves and currents.

Nonlinearities either in loading or in structural systems introduce complications in damping estimations. Nonlinearity effects in combination with nonstationary features of full-scale observations under winds may affect the accuracy of conventional damping estimation procedures (Jeary, 1992). Nonlinearity either in loading, or in a structural system that may couple two orthogonal modes with equal frequencies can add indirectly to the damping available in a system as energy transfers from one direction of motion to another as in a beating mode (Kareem, 1982). This feature in

design can indirectly help to augment damping in buildings provided the two orthogonal modes have the same frequency.

This paper examines types of damping sources available to structures and their modelling and treatment of uncertainty in damping estimates for practical applications.

2. Structural damping

Typically in engineering practice a viscous damping model is used for the sake of simplicity as it lends to a linear equation of motion. The viscous damping coefficient is either assigned on the basis of the material of construction, e.g., steel or concrete, or it is evaluated using a system identification technique. A logarithmic decrement of a free vibration test is one such approach. Any source of nonlinearity is obscured in this approach and consequences of such an assumed model are either ignored or disregarded. This concept has been extended to represent equivalent viscous damping, whereby the energy dissipated by a nonlinear system in a steady-state vibration is equated to the energy dissipated by an equivalent viscous system.

2.1. Damping models

Some of the commonly used damping models can be described by

$$f_d(x, \dot{x}) = a\dot{x}\,|\dot{x}|^{\theta-1}, \tag{1}$$

where $f_d(x, \dot{x})$ is the damping force and a is the damping coefficient. The value of θ determines the damping model, e.g.,

linear viscous damping ($\theta = 1$)

$$f_d(x, \dot{x}) = c\dot{x}; \tag{2}$$

Coulomb damping ($\theta = 0$)

$$f_d(x, \dot{x}) = \mu\frac{\dot{x}}{|\dot{x}|} = \mu\,\mathrm{sign}(\dot{x}); \tag{3}$$

quadratic damping ($\theta = 2$)

$$f_d(x, \dot{x}) = q\dot{x}\,|\dot{x}|. \tag{4}$$

The ratio of the equivalent viscous damping for these cases is given by

viscous damping

$$c/2m\omega; \tag{5}$$

Coulomb damping

$$\frac{2\mu}{\pi m\omega^2 A}; \tag{6}$$

quadratic damping

$$4q\frac{A}{3\pi m}; \tag{7}$$

general nth power damping

$$\frac{1}{2}\frac{a}{m}\gamma(A\omega)^{\theta-1}, \tag{8}$$

where

$$\gamma = \frac{2\Gamma(\frac{1}{2}(\theta+2))}{\sqrt{\pi}\,\Gamma(\frac{1}{2}(\theta+3))},$$

$\Gamma(\ )$ denotes the Gamma function, c is the viscous damping coefficient, q the quadratic damping coefficient, μ the Coulomb damping coefficient and A the amplitude of motion.

It is important to note that the linear viscous damping ratio is independent of amplitude, whereas Coulomb and quadratic damping ratios are inversely and directly proportional to amplitude of motion. For a lightly damped system, where all three preceding damping mechanisms may be present, a first-order approximation for the total damping present in the system can be obtained by fitting data to Eq. (1). Such a model may bring out useful information regarding the inherent damping mechanisms in a system which experiences different types of damping sources, e.g., an offshore platform, or a building whose damping is amplitude dependent. Novak (1971) offers a number of techniques to quantify parameters of nonlinear vibration systems.

Estimates of the model parameters are obtained by a least square fit of the data. Other models such as "stick-slip" type models, elasto-plastic and bilinear models can be invoked to describe the variation of system damping with amplitude. In the case of steel buildings such models can describe the dissipation of energy in frictional modes, e.g., in-filled panels and partitions and between structural framing and cladding. In the case of concrete structures, for uncracked state purely viscous damping occurs. For cracked cases both frictional damping, due to friction between the concrete and reinforcement steel in the cracked tension zone, and viscous damping in the compression zone are present. A concrete element may be modelled by a spring oscillator with viscous dashpot and a stick-slip element.

2.2. Full-scale measurements

The selection of an appropriate value of damping is a subject of controversy in design practice. The present state-of-the-art in the design of tall buildings is such that

it is difficult to predict structural damping closer than plus or minus 30% until the building is completed. This is essentially ascertained on the basis of the knowledge gleaned from existing buildings of similar material and structural systems on which tests have been conducted. Although it is generally agreed that damping values change with amplitude of motion, their fundamental description are rather uncertain and limited. Besides the complex nature of damping mechanisms, the methods employed to ascertain damping of full-scale structures and the analysis and interpretation of data introduce additional uncertainty. Assessment of damping in full-scale structures has been undertaken by several investigators. A sampling of such studies can be found in Jeary and Ellis (1981), Yokoo and Akiyama (1972), Hudson (1977), Hart and Vasudevan (1975), Taoka et al. (1975), Raggett (1975), Celebi and Safak (1992) and Trifunac (1972). Information available from full-scale experiments has been assembled by Haviland (1976), Jeary and Ellis (1981), Yokoo and Akiyama (1972), Davenport and Hill-Carroll (1986), Jeary (1986), Lagomarsino (1993) and Tamura et al. (1994), among others.

Haviland (1976) reported a wide range of data for different levels of response amplitudes, wide classes of structural systems and building heights. This study showed that the log-normal and Gamma distributions provided the best fit to the damping variations. The coefficient of variation (COV) of damping estimates based on his data set varied in the range of 42–87%. Davenport and Carroll (1986) reexamined the data base and noted that the COV ranged from 33% to 78% and suggested a value of 40%. Based on measured data, ESDU (1983), Jeary (1986), Logomarsino (1993) and Tamura et al. (1995) established expressions for damping ratio variation as a function of structural displacement level. It is important to note that most of these data bases have a large overlap of information since they have many common buildings.

A review of the data base that has led to carefully selected expressions for damping variation as a function of amplitude suggests that the data contained therein mostly concerns mid-rise buildings in the vicinity of 20 stories or shorter. However, there is a serious scarcity of data for high-rise buildings taller than 20 stories especially for the level of amplitudes not related to earthquake-induced response which generally provide much higher damping estimates than those available for wind excited structures. More importantly, it is above this range of height where the wind excited resonant part of structural response begins to dominate the background (nonresonant part). Needless to mention, it is the resonant response component that is influenced by damping for which we do not have much information. In Davenport and Carroll (1986) a summary of damping estimates versus amplitudes clearly demonstrates the point made earlier regarding the scarcity of data. In their database for buildings over 20 stories, damping estimates are available at acceptable levels of motion from human comfort considerations and some data points are present for the transition region where the building height determines the level of acceptability. However, not a single data set exists for acceleration levels which are not acceptable with a mean recurrence interval of 10 years. It is the last two levels of motion that are of interest to the designer of tall buildings. A similar difficulty with lack of information of buildings with periods larger than 3 s exists in the data set reported by Lagomarsino (1993). Jeary (1986) very carefully scrutinized the damping data base and eliminated a majority of the measured

damping data due to concerns ranging from lack of documentation to absence of variance errors and confidence intervals. The remaining data base which was used for developing the model was again biased toward mid-rise buildings with the exception of the Transamerica building. The predictor model, however, agrees well with the general conception that the damping values reduce with increasing building height or period. The model due to Lagomarsino (1993) exhibits an opposing trend in that a larger period results in larger damping. With a few notable exceptions, this contradicts most full-scale measurements reported in the literature.

2.3. Damping in higher modes

Damping in the fundamental mode is very low, which indicates that very little energy is dissipated by structural connections and most of the building structure deforms as a rigid body. However, it is expected that in higher modes a building experiences more flexural and shear deformation which may contribute to higher damping. Also, radiation damping due to soil–structure interaction may contribute to higher damping (Novak, 1974). In light of the difficulties with the availability of data and its reliability for damping in the fundamental mode, information on damping in higher modes becomes even more scarce and less reliable. However, for estimating building acceleration to appraise serviceability limit states, the contribution of higher modes must be included. Kareem (1981a) has noted that for the across wind acceleration response of a square cross-section building, the contribution of the second mode is about 13%. Neglecting such contributions may impact the serviceability of a building. O'Rourke (1976), in his discussion of the paper by Saul and Jayachandran (referenced in O'Rourke) concerning the importance of modes vis-a-vis the total acceleration response, examined values of damping in higher modes. Saul and Jayachandran assumed lower damping in higher modes in comparison with the first mode which may have resulted in overemphasizing the relative importance of higher modes. O'Rourke analyzed the data available in the literature and noted that based on the data selected 61% of the cases the damping in the second mode was higher than the damping in the first mode, the corresponding value for the third mode was found to be 53%. The average value of the ratio of second to first mode damping was 1.39 and for the ratio of the third to the first was 1.61. Unlike Saul and Jayachandran's assumption, Kareem (1981a) assumed damping to be proportional to stiffness which increases in higher modes. Accordingly, the damping in higher modes was given by

$$\frac{\varsigma_n}{\varsigma_1} = 1 + C\left(\frac{f_n}{f_1} - 1\right), \tag{9}$$

where C is a constant approximately equal to 0.38 based on the data available in Yokoo and Akiyama (1972) and f represents frequency in the mode given by the subscript. In Fig. 1, the data base from the study by Tamura et al. (1994) and other sources was utilized to examine the applicability of the expression in Eq. (9) in light of the additional data. The data base is restricted to steel buildings of height greater than 20 stories under light to moderate levels of oscillations generally experienced in

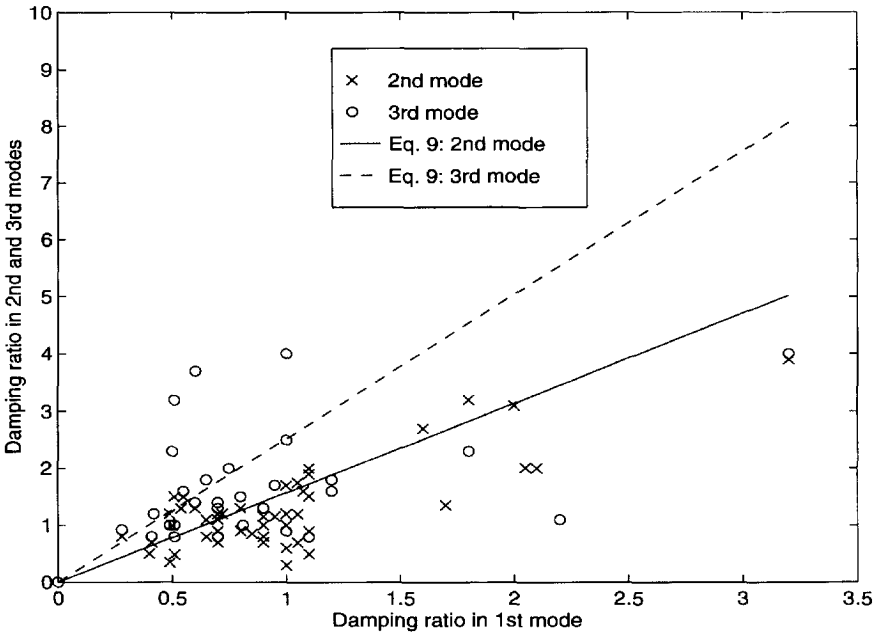

Fig. 1. Damping data base and application of Eq. (9).

typical wind conditions. In view of the general variability of damping which is further compounded by the higher modes, the expression in Eq. (9) appears to portray a satisfactory representation of the general trend.

3. Aerodynamic damping

The equation of motion of an aerodynamically excited structure is given by

$$M\ddot{X} + 2\omega M\zeta_s\dot{X} + M\omega^2 X = F(t, X, \dot{X}, \ddot{X}). \tag{10}$$

The left-hand side of the equation represents typical inertial damping and stiffness forces acting on the structures, whereas the right-hand side of the equation denotes the aerodynamic forcing function which is dependent on time, space and its derivatives. Typically the $\ddot{X}$ and the X are known to have insignificant influence on building response due to the relatively small value of the aerodynamic mass and stiffness in comparison with that of the building. It is the $\dot{X}$ term which depending on its sign contributes positive or negative values of aerodynamic damping on structures. Since the aerodynamic damping is due to building motion, it is manifested in the alongwind, acrosswind and torsional directions. There are two approaches to quantify aerodynamic damping, namely, quasi-steady or unsteady aerodynamics of buildings. These are described below.

3.1. Quasi-steady aerodynamics

The evaluation of aerodynamic damping has been made for a long time with respect to the galloping phenomenon. The concept of quasi-steady theory is invoked. It essentially implies that for every instant during the oscillations, the aerodynamic force is the same as the force on a rigid segment of the body at the same angle of attack. This assumption has been shown to hold good for large reduced velocities where the wavelengths associated with the frequencies of aerodynamic loading are several times the representative width of the building. In this situation, the approach flow can be assumed to be locally steady. The aerodynamic damping on a segment of a building is determined from sectional aerodynamic characteristics for the corresponding angle of attack in terms of a force coefficient and relative velocity. The aerodynamic damping in lateral and torsional directions based on the quasi-steady theory are given by

$$\xi_x^a = \frac{3}{4\pi(3+\alpha)} \frac{\gamma_a}{\gamma_b} \frac{V_n}{f_x d} C_{F_x}, \qquad \xi_y^a = \frac{3}{8\pi(3+\alpha)} \frac{\gamma_a}{\gamma_b} \frac{V_n}{f_y d} \frac{\mathrm{d}C_{F_y}}{\mathrm{d}\theta},$$

$$\xi_\theta^a = -\frac{3}{8\pi(3+\alpha)} \frac{\gamma_a}{\gamma_b} \frac{V_n}{f_\theta d} \frac{rb}{r_m^2} \frac{\mathrm{d}C_{F_\theta}}{\mathrm{d}\theta}, \tag{11}$$

where α is the power law exponent, γ_a, γ_b are the air and building specific weights, C_{F_x}, C_{F_y} and C_{F_θ} are force coefficients in the x, y, θ directions, f_x, f_y, f_θ are the natural frequencies in their respective subscript directions, d is the body width, r is the distance of the leading edge from the building centroid, and r_m is the mass radius of gyration (Kareem, 1978). The preceding expressions utilize linear mode shapes in all three directions.

As noted earlier, the quasi-steady theory is generally not applicable in the low reduced velocity range applicable to the operational velocities of typical buildings in wind. Therefore, the evaluation of aerodynamic damping must be based on unsteady aerodynamics. This can be accomplished through a free oscillation or forced oscillation test.

3.2. Unsteady aerodynamics

The importance of evaluating the aerodynamic damping has increased with the advent of so called aerodynamic models or those utilizing high-frequency base balances. Although there have been a number of reported studies concerning the measurement of aerodynamic loads on structures using a wide variety of force balances, Saunders and Melbourne (1975) were first to carry out a measurement program that resulted in a host of force spectra acting on a wide range of building cross-sections. They also concluded that the nondimensional cross-wind force spectra on the types of buildings tested were insensitive to the level of motion of the buildings for reduced velocities up to at least ten. In other words, the aeroelastic effects, or aerodynamic damping could be neglected. Kareem (1978) noted in a validation study concerning the crosswind spectra derived from statistical integration of surface

pressures that the response estimates computed by using the measured spectra began to depart from the estimated values based on aeroelastic model test of the same building at reduced velocities above 6. The predicted values of response for reduced velocities greater than 6 tended to under-predict the aeroelastic measurements. This suggested that a contribution from the motion-induced effects was missing as it had automatically been accounted for in the aeroelastic case. The damping estimates from the aeroelastic model suggested a constant increase in the negative aerodynamic damping. By including the negative aerodynamic damping, the response predictions provided a better comparison with the aeroelastic tests at higher reduced velocities, but at intermediate reduced velocities some discrepancies remained unresolved (Kareem, 1982). It appears that simply attributing all motion-induced effects to aerodynamic damping may be an excessive simplification. Indeed the motion of a structure also modifies the flow field around it and tends to enhance particularly the spanwise pressure correlation which may lead to an increased forcing in comparison with that measured by a force balance.

Following the work of Saunders and Melbourne (1975), Kwok and Melbourne (1981) reported that at close to the critical reduced velocity and particularly at low values of structural damping, displacement dependent lock-in excitation was found to be significant which resulted in large increases in crosswind response. They suggested inclusion of a sinusoidal lock-in excitation model along with a random excitation model to account for the preceding observation. It was suggested that the lock-in effects become important when the ratio of the building top displacement to its width exceeds 0.025.

Boggs (1992) reported a systematic study that focussed on the validation of aerodynamic model. Although this topic had been addressed earlier, but the relevant error-controlling parameters had not been clearly identified, nor had quantitative limits required for valid results on the parameter studies been established. This study, though limited to a slender square building, has provided a clear picture of the consequences of neglecting aeroelastic feedback and define conditions when an aerodynamic model is valid. The normalized tip deflection criterion was noted to be a poor indicator of aeroelastic magnification and the existence of such a critical limit is not justified. Results of this study show that the reduced velocity, in conjunction with the mass damping parameter, provide a good characterization of the aeroelastic magnification factor given by the ratio of the response estimate by aeroelastic model and the aerodynamic model. Bogg's results demonstrate that for the mass damping parameter in the range of typical tall buildings the motion-induced effects may be worth consideration for reduced velocities as low as 6. This corroborates observation made by Kareem (1982).

3.3. Experimental identification of aerodynamic damping

Experimental identification of aerodynamic forces can be accomplished either by a free vibration or a forced vibration test. In the free vibration case, the change of frequency and damping of models oscillating in wind are observed. This method has been extensively used to identify motion-dependent aerodynamic forces in bridge

aeroelasticity (Scanlan and Tomko, 1971). Kareem (1982) has utilized a free vibration approach to assess the aerodynamic damping of building models and chimneys in the wind tunnel. A number of researchers have utilized forced vibration tests to identify aerodynamic stiffness and damping of two-dimensional models (e.g., Otsuki et al., 1974). Steckley (1989) used an experimental system for the measurement of motion-induced forces on a base pivoted model. This study cataloged variation of the motion-induced force with oscillation amplitude for prisms of different cross-section. This data was later employed by Watanabe et al. (1995) to fit empirical aerodynamic damping functions for practical applications. Their model is based on real and imaginary parts of the modified complex transfer function of a single degree of freedom (SDOF) oscillator.

4. Hydrodynamic damping

In the case of offshore systems in addition to the structural and aerodynamic fluid damping discussed above, the damping due to hydrodynamic effects provides an important contribution to the structural response.

The sources of hydrodynamic damping are generally radiation and drag induced effects. For the large majority of offshore structures, the drag-induced component of hydrodynamic damping is the dominant contributor. The magnitude of the drag-induced damping is dependent on the drag coefficient used in the Morison equation, which expresses hydrodynamic force as a function of relative fluid-structure velocity and acceleration as in

$$F_H = f(a) + \tfrac{1}{2}\rho_w C_{Dw} A_w (u - \dot{X})|u - \dot{X}|, \tag{12}$$

where a, u are the water particle acceleration and velocity, ρ_w, A_w are the water density and the frontal area of the immersed system, and C_{Dw} is the underwater drag coefficient. The negative force due to the minus sign in the last term above provides the hydrodynamic damping. The damping coefficient is dependent on the size of the structure with respect to the wavelength of the incoming wave field, and is generally determined experimentally.

Depending on the structural size to wavelength ratio the drag mechanism may exhibit both linear and quadratic dependence on relative fluid-structure velocity. For frequency domain analysis the linear term is treated in a straightforward manner, while the quadratic term may be expressed through an equivalent linearization approach. The total system damping is expressed as the sum of its components

$$\xi = \xi_S + \xi_A + \xi_{W_1} + \xi_{W_2}, \tag{13}$$

where the subscripts S, A, W_1, W_2 indicate structural, aerodynamic, and first and second order hydrodynamic terms. Now, the linear hydrodynamic term is given as

$$\xi_{W_1} = \frac{\gamma \rho_w \pi h \sqrt{v \sum D_i}}{m\sqrt{4\pi f_n}}, \tag{14}$$

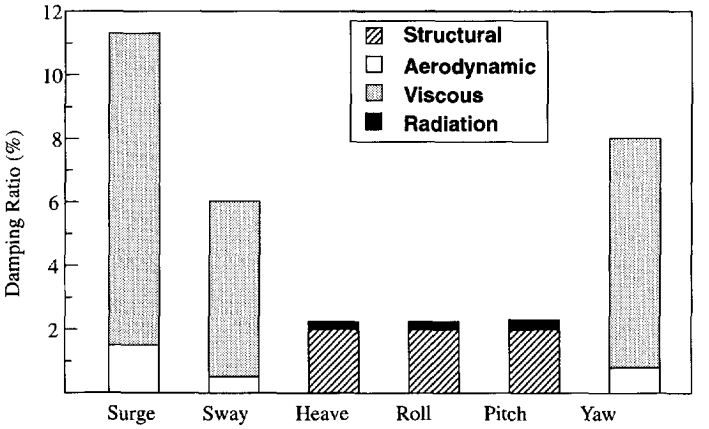

Fig. 2. Damping components for a TLP.

where h is the draft of the structure, v is kinematic viscosity, $\sum D_i$ is the sum of the diameters of the underwater portion of the structure, f_n is the natural frequency of the system, m is the system mass, and γ is unity for Stokes damping, and larger for turbulent fluid. The quadratic hydrodynamic damping term is

$$\xi_{W_2} = \frac{\rho_w C_{Dw} A_w \sigma_u}{4(2\pi f_n)m}\left[\left(2\sqrt{\frac{2}{\pi}}\right)\exp\left(-\frac{\bar{U}_c^2}{2}\right) + 2\bar{U}_c^2\,\mathrm{erf}\left(\frac{\bar{U}_c}{\sqrt{2}}\right)\right], \tag{15}$$

where $\bar{U}_c$, σ_u are the mean current velocity and the r.m.s. water particle velocity in the waves.

4.1. Example

Currents, wind and waves all contribute to the nominal surge damping of a tension leg platform (TLP). The damping sources include viscous, radiation, aerodynamic and structural effects. For the motion in the horizontal plane, the viscous damping has the most significant contribution to the overall damping (Fig. 2). The radiation damping is negligible, but the aerodynamic damping which is often neglected should be included for an accurate prediction of the response. In the presence of currents, the viscous damping ratio would be as large as 30%, and in such cases it dominates any other damping source for the motion in the horizontal plane.

5. Evaluation of damping

Damping estimation from a time history of response can be classified into two categories: spectral and time-series approaches. In this paper, auto-correlation decay, logarithmic decrement, spectra based half-power method, spectral moment method,

random decrement method, spectral curve fitting, and wavelet transform based spectral estimates are classified as spectral approaches. The time-series techniques are those related to methods of time-series analysis, i.e., maximum entropy estimates, auto-regressive (AR), or auto-regressive and moving averages (ARMA).

5.1. Spectral techniques

The infinite harmonic basis functions in Fourier based spectral estimation necessarily introduce errors when applied to finite duration signals. Most spectral-based approaches have difficulties providing sufficient accuracy because of limitations on resolution and high coefficients of variation (COV) of spectral estimates as longer data sets are needed to improve estimates. By increasing degrees of freedom, either by merging neighboring spectral estimates, by ensemble averaging the individual estimates from several realizations, or both, spectral estimates can be improved, but this approach is marred by the unavoidable presence of nonstationarity concerns inherent with long records. Details concerning this issue in the literature abound. In view of the preceding difficulty, attempts to smooth the actual spectral estimates have been made through curve fitting. For example, the fitting of spectral estimates to a transfer function of a SDOF system by employing maximum likelihood estimator and a least squares approach can be found in Breukelman et al. (1993) and Jones and Spartz (1990), respectively. By selection of a sample length long enough to ensure sufficient frequency resolution, avoiding nonstationarity problems and by ensemble averaging of similar records to reduce variance of spectral estimates good smoothed spectra for linear systems can be obtained. However, the characteristic features of nonlinear systems, with transfer functions that depart from linear, and the response of systems to nonlinear loading may be obscured in such a curve fitting approach. Similar observations have been made by Jeary (1992).

Wavelet-based spectral estimation offers another alternative, as it better represents the true signal energy due to the use of localized basis functions (Gurley and Kareem, 1995). It is shown in Gurley and Kareem (1995) that the wavelet estimator exactly reproduces the signal energy which the Fourier-based spectral estimate does not reproduce due to leakage that results in raggedness in the spectral curves. The use of orthogonal wavelets provides the spectral estimates, especially at the high frequencies with resolution that is not as good as that obtained in Fourier-based approaches. However, at very low frequencies the wavelet-based estimates give much better resolution. This can be further improved by spectral estimation within an octave by over-sampling which leads to nonorthogonal wavelets or by a zooming technique (Gurley and Kareem, 1995).

In a later section, the efficacy of the random decrement method for estimating damping will be evaluated through examples.

5.2. Time-series methods

The methods based on a time-series approach offer advantages over spectral methods as they eliminate the problems of resolution based on short length of records

as well as questions about the stationarity of long records. These spectral estimates provide smoother curves without the leakage problems associated with the Fourier-based approaches. The leakage problems are significant for short length data sets where the uncertainty principle does not permit good frequency resolution. The time-series methods are sensitive to the order of the model or the number of coefficients (Li and Kareem, 1990, 1993). In the case of an AR model if the order is small then the dominant peaks may not be resolved, whereas, large-order systems may introduce spurious peaks which may contaminate the spectral estimate as well as the variance. An optimal selection of the order results in accurate spectral estimates.

A serendipitous advantage of these time-series-based models is that the spectrum as well as the time series are estimated once the model coefficients are known. Furthermore, the estimates of structural characteristics is also possible from system identification techniques using time-series models, e.g., ARMAX models (auto-regressive moving average model with exogenous input). In such a case, the system is modelled by an input, output, and noise. The modulus and argument of the poles of the system transfer function are related to system damping and frequency (e.g., Safak, 1989).

5.3. *Random decrement method*

This method utilizes the resulting signature from the ensemble averaging of segments of the response of a linear system to determine system damping. The requirement of specific initial conditions for each segment in the averaging procedure yields a signature which represents free vibration of the system from an initial displacement. Damping estimates are then extracted from this free vibration signature (Cole, 1973). The response of a dynamic system is a superposition of the response due to both displacement and velocity initial conditions, and the forced vibration response

$$x_T = x_{x_0} + x_{\dot{x}_0} + x_F. \tag{16}$$

The goal is to ensemble average samples of response data such that the initial velocity response and forced vibration response components reduce to zero.

The forced vibration response of a linear system due to a zero mean stationary random input is itself random zero mean stationary. As the number of segments increases, the ensemble average of such a process tends to zero. If all segments in the average begin at the same threshold level x_{th} and alternating positive and negative slope, then the response due to initial velocity is averaged out while the response due to initial displacement at x_{th} remains. The random decrement method is demonstrated in principle in Fig. 3, where the components of the signal are ensemble averaged separately to illustrate the progression of the signal from a forced vibration to a free vibration decay.

The random decrement signature $\eta(t)$ is expressed as (Yang et al., 1983)

$$\eta(\tau) = \frac{1}{N} \sum_{i=1}^{N} x_i(t_i + \tau), \tag{17}$$

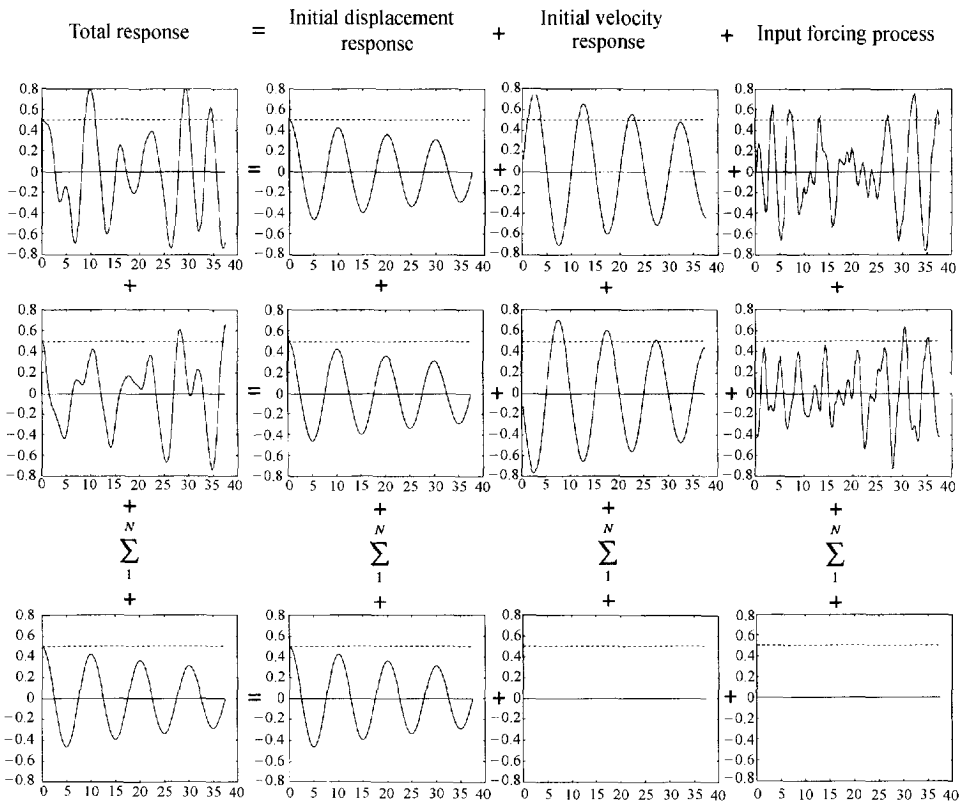

Fig. 3. The random decrement technique.

where $x_i(t_i)$ is the threshold value and, the initial slope flips for each sequential segment. The random decrement signature is defined in the time interval $0 \leqslant \tau \leqslant \gamma$ where γ is the time from the starting point of the last segment to the end of the signal. N is the number of segments in the ensemble average.

This intuitive explanation has been used in much of the available literature, and seems to be reasonable for linear systems. The technique has an advantage over the use of autocorrelation or spectral methods in that it is not encumbered by the limitations concerning input amplitude and resolution, respectively. Some researchers have found the method suitable for systems with nonlinear damping characteristics (e.g. Jeary, 1992). However, the number of segments needed in the ensemble may be quite high in order to produce a repeatable signature, thus a large data set is required.

The conclusion that the resulting signature is the free vibration decay of the system does provide reasonable damping estimates in many cases. However, it has been shown (Vandiver et al., 1982) to be mathematically incorrect. Specifically, the requirement of a uniform value for the initial condition of each segment biases the expected value of the excitation, and the last term in Eq. (16) is not necessarily zero in the

average. The solution to the equation of motion is given by

$$x_T(t) = x_0 e^{-\xi\omega_n t}\left(\cos\omega_d t + \frac{\omega_n}{\omega_d}\sin\omega_d t\right) + \frac{\dot{x}_0}{\omega_d} e^{-\xi\omega_n t}\sin\omega_d t + \int_0^t h(t-\tau) f(\tau)\,d\tau, \tag{18}$$

where $\omega_n = \sqrt{k/m}$, $\omega_d = \omega_n\sqrt{1-\xi^2}$, x_0 and $\dot{x}_0$ are the displacement and velocity initial conditions, and $h(t)$ is the system impulse response function.

The random decrement signature is the expected value of Eq. (18) conditioned by the initial values of each segment in the average as in

$$E[x_T(t)|x_0, \dot{x}_0] = x_0 e^{-\xi\omega_n t}\left(\cos\omega_d t + \frac{\omega_n}{\omega_d}\sin\omega_d t\right) + E\left(\frac{\dot{x}_0}{\omega_d} e^{-\xi\omega_n t}\sin\omega_d t\right) + \int_0^t h(t-\tau) E[f(\tau)|x_0, \dot{x}_0]\,d\tau. \tag{19}$$

The first term on the right-hand side is not affected by the expected value operator, and gives the free vibration response to an initial displacement. The magnitude of the second term on the right-hand side is the same with alternating sign over an even number of samples, which averages to zero. The expectation in the third right-hand term, according to the intuitive theory, vanishes, since $f(t)$ is a random zero mean process. However, since it is conditioned by the requirement of x_0 and $\dot{x}_0$, it is not in general zero. Thus the intuitive interpretation of the random decrement signature as the free vibration response is not correct (Vandiver et al., 1982).

For the case where the excitation is stationary Gaussian white noise, the autocorrelation of the response of a SDOF system is proportional to its free vibration response. For most applications, random decrement is applied to narrow-banded systems with relatively wide-banded excitation (e.g. building response to buffeting effects of wind). For such cases a white noise approximation is acceptable, and the intuitive explanation is appropriate, though not rigorously correct.

The resultant signature for a linear system under Gaussian stationary input is proportional to the autocorrelation of the system response, and is expressed as (Vandiver et al., 1982)

$$\eta(t) = E[x_T(t)|x_0, \dot{x}_0] = \frac{R_x(\tau)}{R_x(0)} x_0, \tag{20}$$

with a variance of

$$\mathrm{Var}[\eta(t)] = \frac{1}{N} R_x(0)\left(1 - \frac{\eta^2(t)}{x_0^2}\right). \tag{21}$$

Where it is seen from Eqs. (20) and (21) that the variance is independent of the threshold level x_0, since it is assumed that there is no noise in the measured signal. If noise exists, the variance should increase with decreasing threshold levels.

Several examples of the application of the random decrement method are now shown. The data set for the first two examples is the response of a model TLP subjected to wind and wave loads, and has a bimodal spectrum. The response of systems with more than one well-separated mode must be band-pass filtered about the desired mode in order to apply the random decrement method. First, the low frequency mode is analyzed by low-pass filtering the data. The lengths of the data records proved to be too short to generate a repeatable signature. That is, the signature should give the same damping estimate regardless of the user selected constant value at which segments are initiated. Fig. 4 shows several random decrement signatures for the same system response. The signatures vary drastically from case to case, and a consistent damping estimate cannot be made among them. Notice also that the signatures do not resemble a free vibration decay signal.

The recommended number of segments is 400 to 500 according to some researchers (Yang et al., 1983), while others recommend at least 2000 (Tamura et al., 1992). The above records have 6000 data points at most, and for the low frequency mode this included about 50 complete cycles. Each cycle can produce two segments for the

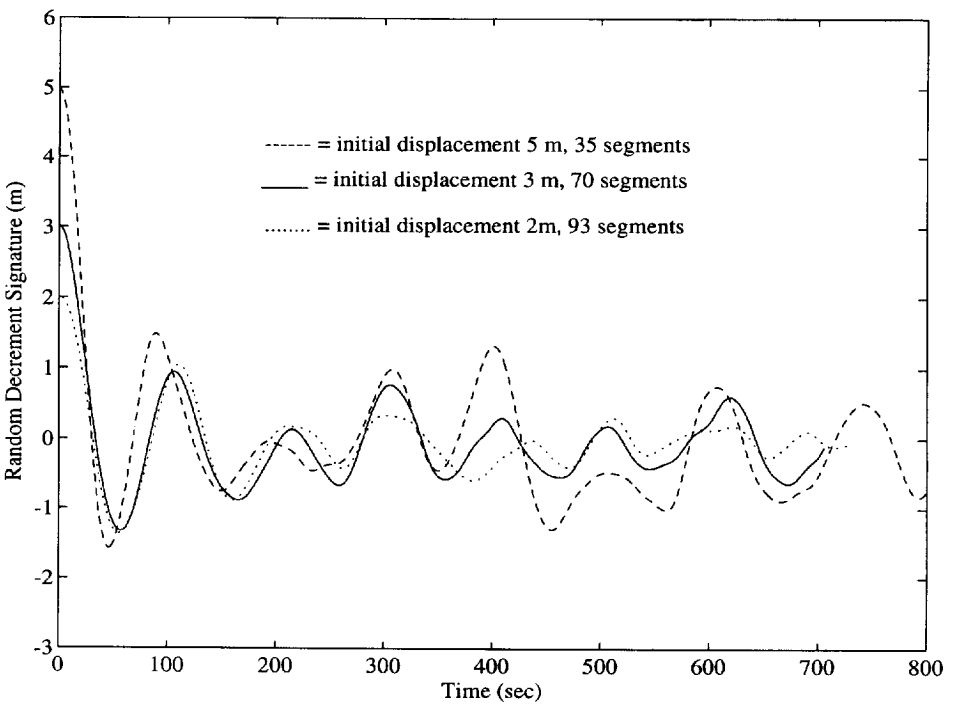

Fig. 4. Random decrement signature of low frequency response of an offshore platform.

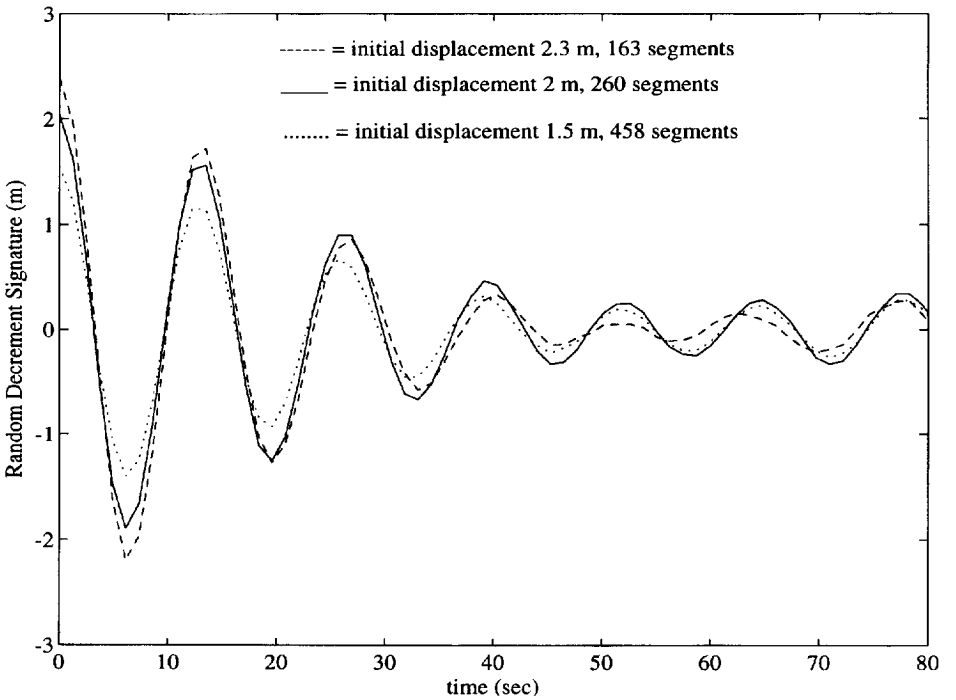

Fig. 5. Random decrement signature of wave frequency response of an offshore platform.

ensemble average, but 100 segments is not enough to sufficiently average out the random components of the response. In addition, the low frequency response is nonlinear, which violates the assumption of superposition of the response components.

The response of the platform also has a mode corresponding to the natural frequency of the incoming wave field. At the wave frequency, many more cycles are present in data recorded than for low frequency oscillation. This allows for more segments to be averaged when acquiring a random decrement signature. Fig. 5 shows the random decrement signature for this higher frequency linear response to the wave field. The number of segments range from 163 to 458. These signatures are much more consistent with each other, and more closely resemble a free vibration decay signature. The response at the wave frequency is linearly related to the input wave elevation, which corresponds with the assumption of superimposed responses. This signature may be used to estimate damping at this mode, but there is no exact value of damping to compare the estimate with.

In order to evaluate the applicability of the random decrement method to the above example, the response of a linear oscillator with a natural undamped frequency of 0.35 Hz and known damping to a wave train is numerically simulated at a sampling rate of 4 Hz. The random decrement signature is then used to estimate the known

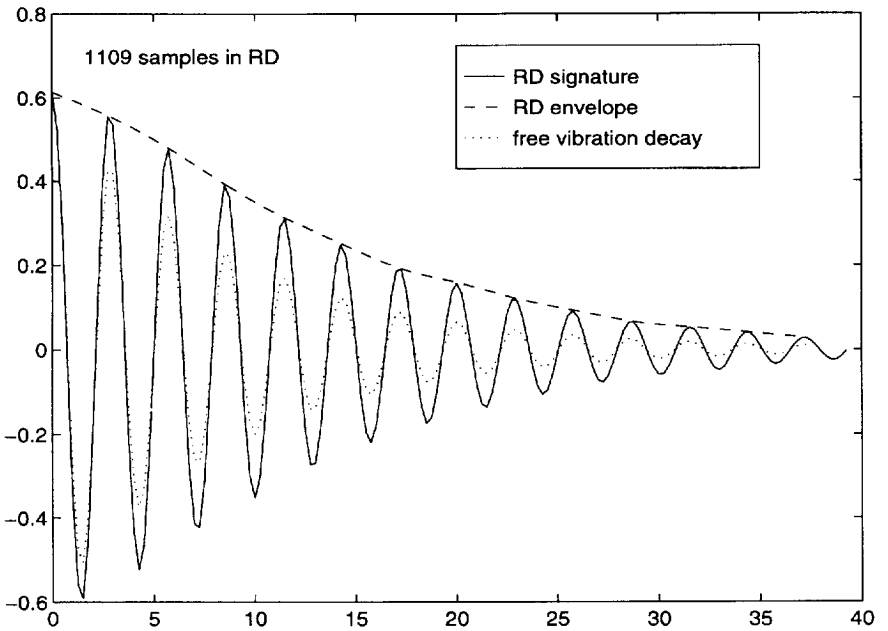

Fig. 6. Random decrement and free vibration decay response of linear oscillator under colored noise.

damping value. A JONSWAP sea spectrum is applied to produce a linear wave train from standard frequency domain simulation techniques. The sea state used is fairly wide-banded, with a peakedness parameter of 1.0, and the system frequency is set at the peak of the input spectrum in order to better facilitate the white noise approximation. Fig. 6 shows the random decrement signature of the oscillator response using 1109 overlapping segments with an initial displacement at each segment of 0.6. The known damping is 5% of critical, while the damping estimates from the signature using the logarithmic decrement and half-amplitude methods are 2.9% and 3.1%, respectively. Several threshold values were selected as initial displacement conditions in different runs, resulting in a consistent underestimation of the damping from 15% to 40%. Fig. 6 also shows the actual free vibration response of the oscillator with an initial displacement equal to the corresponding threshold value. It is clear that the random decrement signature does not decay as quickly as the corresponding free vibration response.

The same oscillator is subjected to white noise excitation with the same energy level as that of the above wave train in the range of the system natural frequency. The resulting signature from 1109 overlapping segments with a 0.6 threshold value and the corresponding actual free vibration decay are shown in Fig. 7. The estimated damping values are 5.3% and 4.9% for the logarithmic decrement and half-amplitude methods respectively. The damping estimates and the results in Fig. 7, in comparison with those in Fig. 6, demonstrate the importance of applying a white noise or wide-banded

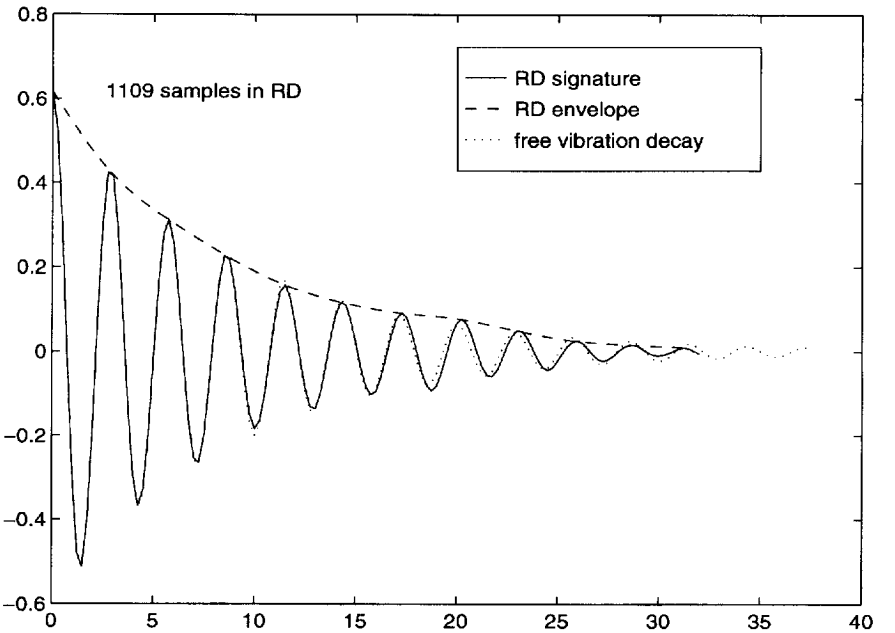

Fig. 7. Random decrement and free vibration decay response of linear oscillator under white noise.

input process in order to validate the application of the random decrement method.

The effects of violating the linear system assumption are investigated by replacing the linear oscillator with a nonlinear softening oscillator. This system is subjected to the same white noise input as the previous example. Fig. 8 shows the resulting random decrement signature and free decay of the nonlinear oscillator using 1109 segments as before. The damping estimates are 5.5% and 5.2% for the logarithmic and half-amplitude methods respectively. It is noted that the frequency of the signature departs from that of the free decay as the amplitude decreases in the record. This will effect the damping estimate depending on the particular cycles used for the damping estimation techniques. Here, they are the same as the previous examples. The estimates are comparable to those of the linear system, however, they are not robust with respect to the selected threshold value and selected cycles for the applied techniques, as they were found to be for the linear system. Varying the threshold value from 0.3 to 0.8 for the linear system provides averaged damping estimates from the two methods in the range of 4.5% to 5.2%. For the nonlinear system the estimates range from 4.4% to 5.8%, and show a wide degree of scatter.

The technique is next compared with the spectral damping estimation approach using the half-power bandwidth method. The response record of the linear oscillator subjected to white noise is segmented into 64 segments of 512 points each. These segments are windowed and the power spectral density is estimated using standard

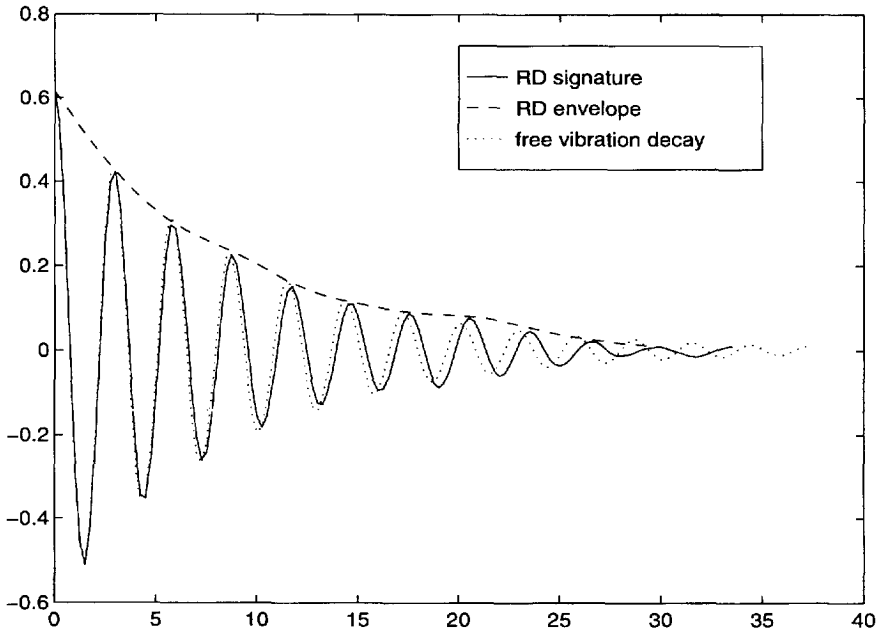

Fig. 8. Random decrement and free vibration decay response of nonlinear oscillator under white noise.

FFT methods. The half-power bandwidth method estimates the damping at 3.8%, an underestimation of 24%. A longer data record may well provide better estimates by adding resolution to the spectrum, but the random decrement method closely predicts damping with the current record length, as demonstrated above.

This method is well suited to the response of structures under buffeting wind loading, where the spectrum of the input process is wide-banded. However, wind forces which are the result of vortex shedding are narrow-banded in nature, leading to the same difficulties experienced in the above colored noise example.

6. Uncertainty analysis

The treatment of inherent uncertainty associated with damping in structural systems, as alluded earlier, is presented here to incorporate its effect on structural response estimates. A second-order perturbation technique, a second-moment approach, and a Monte Carlo simulation are presented to examine the effects of damping variability on the dynamic response of structures. The damping uncertainty may be expressed in terms of the damping constant, or alternatively, in terms of critical damping ratios. In view of the impracticality of determining damping coefficients and the general engineering practice of expressing structural damping in terms of the critical damping ratio, the analysis reported here is based on the damping ratios.

6.1. Perturbation approach

The equations of motion of a discretized system subjected to an external excitation are given by

$$\underline{M}\underset{\sim}{\ddot{X}} + \underline{C}\underset{\sim}{\dot{X}} + \underline{K}\underset{\sim}{X} = \underset{\sim}{F}(t), \tag{22}$$

in which $\underline{M}$, $\underline{K}$ are assembled deterministic mass and stiffness matrices, $\underline{C}$ is a proportional uncertain damping matrix, $\underset{\sim}{X}$ is the response vector, and $\underset{\sim}{F}(t)$ is the external excitation vector (e.g. wind or wave loading). Employing the standard transformation of coordinates involving undamped eigenvectors $\underset{\sim}{\Phi}_i$ of the system offers the following uncoupled equations:

$$\ddot{q}_i + 2\xi_i\omega_i\dot{q}_i + \omega_i^2 q_i = p_i(t), \tag{23}$$

in which $p_i(t) = \underset{\sim}{\Phi}_i^{\mathrm{T}}\underset{\sim}{F}(t)$ and $\underset{\sim}{X} = \underset{\sim}{\Phi}_i q_i$.

The uncertain damping ratio that corresponds to the ith mode in the previous equations may be expressed in terms of the mean and perturbed values

$$\xi_i = \xi_i^0(1 + \alpha_i), \tag{24}$$

in which ξ_i^0 is the mean value of the damping ratio, and α_i is a small Gaussian fluctuation. In certain physical situations it is possible to experience random fluctuation in damping as a function of time, e.g., in aeroelasticity applications. Uncertainty in damping is propagated using a second-order perturbation technique. The higher-order perturbations are possible in principle, but would require moments of order higher than fifth, involving extensive computations. Following the perturbation approach, the modal response is expressed in terms of the mean and perturbed values

$$q_i = q_i^0 + q_i'\alpha_i + q_i''\alpha_i^2, \tag{25}$$

in which q_i^0, q_i', q_i'' are various orders of perturbation.

Substituting Eqs. (24) and (25) into Eq. (23) and equating the same powers of α_i offers the following zeroth-, first- and second-order equations for externally excited systems.

$$\ddot{q}_i^0 + 2\xi_i^0\omega_i\dot{q}_i^0 + \omega_i^2 q_i^0 = P_i(t), \qquad \ddot{q}_i' + 2\xi_i^0\omega_i\dot{q}_i' + \omega_i^2 q_i' = -2\xi_i^0\omega_i\dot{q}_i^0,$$
$$\ddot{q}_i'' + 2\xi_i^0\omega_i\dot{q}_i'' + \omega_i^2 q_i'' = -2\xi_i^0\omega_i\dot{q}_i'. \tag{26}$$

The transient and steady-state modal response at each order may be obtained following the procedures of random vibration theory. In this paper, only the steady-state response analysis is considered. The interested reader is referred to Kareem and Sun (1989) for other details and seismic analysis.

In the frequency domain, the mean square response of a linear system is given by

$$\sigma_{q_i^{(r)}}^2 = \int_0^\infty |H_{q_i^{(r)}}(\Omega)|^2 S_i(\Omega)\,\mathrm{d}\Omega, \qquad S_i(\Omega) = \{\Phi_i\}^{\mathrm{T}}[S_F(\Omega_i)]\{\Phi_i\}, \tag{27}$$

in which $\sigma^2_{q_i^{(r)}}$ is the variance of the rth order modal response in the ith mode, $|H_{q_i^{(r)}}(\Omega)|^2$ is the squared modulus of the system transfer function, and $S(\Omega)$ is the power spectral density (PSD) of the excitation.

The transfer functions corresponding to Eq. (26) are given here

$$H_{q_i^0}(\Omega) = H_i(\Omega), \qquad H_i(\Omega) = \frac{1}{\Omega^2 + \omega_i^2 + 2j\Omega\omega_i\xi_i^0},$$

$$H_{q_0'}(\Omega) = -2\xi_i^0\omega_i j\Omega H_{q_i^0}(\Omega)H_i(\Omega), \qquad H_{q_i''}(\Omega) = -2\xi_i^0\omega_i j\Omega H_{q_i'}(\Omega)H_i(\Omega). \tag{28}$$

Generally, the integration in the preceding equation is performed numerically. However, for white noise excitation and a class of filtered white noise excitation, closed-form integrals are available (James et al., 1947). Accordingly, the mean square response at various orders is given by

$$\sigma^2_{q_i^0} = \frac{\pi S_i}{2\xi_i^0\omega_i^3}, \qquad \sigma^2_{q_i'} = \frac{S_i A_3 B_1^2}{A_1(A_2A_3 - A_1A_4) - A_0A_3^2},$$

$$\sigma^2_{q_i''} = \frac{\pi S_i a_0 b_3(a_0a_3a_5 + a_1^2a_6 - a_1a_2a_5)}{a_0(a_0^2a_5^3 + \cdots - a_1a_2a_3a_4a_5)}, \tag{29}$$

in which S_i is the amplitude of the mode-generalized external excitation, e.g., wind or wave loading, at the ith modal frequency, and

$$B_1 = -2\xi_i^0\omega_i, \qquad A_0 = \omega_i^4, \qquad A_1 = 4\xi_i^0\omega_i^3, \qquad A_2 = 2\omega_i^2 + 4\omega_i^2\xi_i^{0^2},$$

$$A_3 = 4\omega_i\xi_i^0, \qquad A_4 = 1,$$

$$b_3 = (4\xi_i^{0^2}\omega_i^2)^2, \qquad a_0 = 1, \qquad a_1 = 6\xi_i^{0^2}\omega_i, \qquad a_2 = 3\omega_i^2(1 + 4\xi_i^{0^2}),$$

$$a_3 = 4\xi_i\omega_i^3(2\xi_i^2 + 3),$$

$$a_4 = 3\omega_i^4(1 + 4\xi_i^{0^2}), \qquad a_5 = 6\xi_i^0\omega_i^5, \qquad a_6 = \omega_i^6.$$

The response in the physical coordinates at the nth node is given by

$$X_n(t) = \sum_{i=1}^{M} \Phi_{ni}q_i(t), \qquad X_n(t) = \underset{\sim}{\Phi}^{\mathrm{T}}\underset{\sim}{\theta}, \tag{30}$$

where Φ_{ni} denotes the nth element of the ith mode shape, $\underset{\sim}{\Phi}^{\mathrm{T}} = [\underset{\sim}{\Phi}_n^{\mathrm{T}}\ \underset{\sim}{\Phi}_n^{\mathrm{T}}\ \underset{\sim}{\Phi}_n^{\mathrm{T}}]$, and $\underset{\sim}{\theta} = [\underset{\sim}{q}^0\ \underset{\sim}{\alpha q'}\ \underset{\sim}{\alpha^2 q''}]^{\mathrm{T}}$. The covariance of $X_n(t)$ is expressed as

$$\underline{\Sigma}_{x_n} = \underline{\Phi}^{\mathrm{T}}\underline{\Sigma}_\theta\underline{\Phi}, \tag{31}$$

in which the covariance matrix $\underline{\Sigma}_\theta$ is given by

$$\underline{\Sigma}_\theta = \begin{bmatrix} [E(\underset{\sim}{q}^0\underset{\sim}{q}^{0^{\mathrm{T}}})] & [E(\underset{\sim}{q}^0\underset{\sim}{\alpha q'}^{\mathrm{T}})] & [E(\underset{\sim}{q}^0\underset{\sim}{\alpha^2 q''}^{\mathrm{T}})] \\ & [E(\underset{\sim}{\alpha q'}\underset{\sim}{\alpha q'}^{\mathrm{T}})] & [E(\underset{\sim}{\alpha q'}\underset{\sim}{\alpha^2 q''}^{\mathrm{T}})] \\ \text{symmetrical} & & [E(\underset{\sim}{\alpha^2 q''}\underset{\sim}{\alpha^2 q''}^{\mathrm{T}})] \end{bmatrix} \tag{32}$$

and the operator $E(\ )$ denotes expectation. Assuming independence of α_i and q_i and its components, and utilizing relationships for the higher-order moments of Gaussian processes, the terms in the preceding equation can be evaluated. Some of these terms vanish by virtue of Gaussianity. The contribution of the off-diagonal terms is relatively small in relation to the main diagonal terms. As an approximation, by ignoring them, the mean square value of the response at the nth node is given by

$$\sigma_{x_n}^2 = \sum_i^M \Phi_{ni}^2 [\sigma_{q_i^0}^2 + \sigma_{q_i'}^2 \sigma_{\alpha_i}^2 + 3\sigma_{q_i''}^2 \sigma_{\alpha_i}^4], \tag{33}$$

where σ^2 with a subscript denotes the mean square value of the prescribed variable.

An example is presented to demonstrate the influence of uncertain damping on the along-wind acceleration response of a 100 ft square in plan and 600 ft tall high-rise building. The structural system is lumped at five levels and the associated mass and stiffness matrices are described in Li and Kareem (1988). The modal damping ratios in ascending order are 1%, 1.57%, 2.14%, 2.52%, and 2.95%, respectively. The COV of the modal damping ratio was varied from 10% to 40% with uniform increments of 10% and the mean wind was 100 ft/s at the building height. In Table 1 the r.m.s. alongwind acceleration (mg) at each building lumped node is presented in terms of the zeroth-, first-, and second-order perturbations. The second-order contribution increases concomitantly with an increase in the COV of the damping value.

6.2. *Monte Carlo method*

The concept of gust factors and uncertainty analysis is applied to a TLP to predict its response statistics to wind loading (Gurley and Kareem, 1993). The hydrodynamic damping related to quadratic damping is only considered here. The simulation consists of assigning random values to the various uncertain parameters described

Table 1
r.m.s. acceleration response (mg) to wind excitation

	Node					Ω_ξ (%)
	1	2	3	4	5	
Zeroth-order	0.983	1.705	2.278	2.714	2.987	
First-order	0.998	1.729	2.311	2.753	3.030	10
Second-order	0.998	1.730	2.312	2.754	3.031	
First-order	1.039	1.801	2.407	2.868	3.156	20
Second-order	1.049	1.806	2.414	2.875	3.164	
First-order	1.105	1.915	2.560	3.049	3.356	30
Second-order	1.116	1.936	2.589	3.084	3.394	
First-order	1.191	2.064	2.759	3.286	3.617	40
Second-order	1.222	2.124	2.843	3.387	3.727	

Table 2
TLP uncertainty analysis results

	All uncertainties included		Drag coefficients uncertainties	
	Mean	COV	Mean	COV
Hydrodamping	0.27502	0.12724	0.28154	0.29976
Aerodamping	0.02370	0.09549	0.02370	0.22312
Response	24.825 m	0.29618 m	24.019 m	0.26802 m
Gust factor	1.4683	0.02245	1.4911	0.04671
Wind force 7% probability of exceedence	9.84101e6 N		9.47524 e6 N	

based on their assigned probability density function. The wind field is simulated using an ocean based wind spectrum for the frequency domain based fluctuating response calculation, and a twenty year extreme value distribution based on full-scale ocean measurements is used to simulate the wind speed for the mean response calculation.

Here we present the change in response, damping, gust factor and wind force statistics with a changing number of uncertain versus deterministic parameters. The parameters considered uncertain in the first simulation example are parameters in the input wind spectrum, the natural frequency of the system, the air and water drag coefficients, the turbulence intensity of the incoming wind field, and parameters in the coherence function. In the second simulation all parameters are deterministic with the exception of the drag coefficients in air and water which contribute to aerodynamic and hydrodynamic damping. The results of both simulations are presented in Table 2. It is noted that the effects of the type of uncertainties are dependent on the item of interest due to interdependency of parameters. Additional details can be found in Gurley and Kareem (1993).

6.3. *Second-moment analysis*

The second-moment techniques have provided practical and efficient means of analyzing problems in engineering mechanics. The attractiveness of these techniques rests on the limited statistical information needed to analyze a problem, i.e., only the first two moments. The coefficient of variation of structural response $R = f(X_1, X_2, \ldots, X_n)$ which is a function of a number of variables X_i in the first-order second moment (FOSM) format is given by

$$\Omega_g = \frac{1}{\bar{R}}\left[\sum_{i=1}^{N}\left(\frac{\partial g}{\partial X_i}\bigg|_{\bar{X}_i}\right)^2 \bar{X}_i^2 \Omega_{X_i}^2 + \sum\sum_{i\neq j}\rho_{ij}\left(\frac{\partial g}{\partial X_i}\bigg|_{\bar{X}_i}\right)\left(\frac{\partial g}{\partial X_j}\bigg|_{\bar{X}_j}\right)\bar{X}_i\bar{X}_j\Omega_{X_i}\Omega_{X_j}\right]^{1/2}, \quad (34)$$

in which ρ_{ij} is the correlation between X_i and X_j, Ω_{X_i} is the COV of variable X_i. This concept is utilized to illustrate the influence of uncertainty in acrosswind aerodynamic damping on the response of a chimney via the functional relationships between them.

The aerodynamic damping in the acrosswind direction are given by Basu and Vickery (1983) as follows:

$$\xi_a = -\frac{\rho D_0^2}{M_e}\left[C_1 - C_2\left(\frac{\sigma}{D_0}\right)^N\right], \tag{35}$$

where M_e is the equivalent modal mass per unit length, and C_1, C_2 are functions of the mode shapes and aerodynamic parameters, σ is the response level and D_0 is the chimney diameter. Following the FOSM approach the uncertainty in aerodynamic damping is given by

$$\Omega_{\xi_a} = \frac{1}{\xi_a^2}\left[\left(\frac{\partial \xi_a}{\partial D^*}\right)^2 \Omega_D^2 + \left(\frac{\partial \xi_a}{\partial m^*}\right)^2 \Omega_{m^*}^2 + \left(\frac{\partial \xi_a}{\partial K_{a0}}\right)^2 \bar{K}_{a0}^2 \Omega_{a0}^2 + \left(\frac{\partial \xi_a}{\partial a}\right)^2 \bar{a}^2 \Omega_a^2 + \left(\frac{\partial \xi_a}{\partial \sigma_y}\right)^2 \bar{\sigma}_y^2 \Omega_{\sigma_y}^2 + \left(\frac{\partial \xi_a}{\partial N}\right)^2 N^2 \Omega_N^2\right]^{1/2}, \tag{36}$$

in which K_{a0} is an aerodynamic parameter related to C_1 and C_2 (Kareem, 1988). In Kareem (1988), analysis of a chimney response with 14 uncertain parameters was conducted. Structural damping COV was 0.35. The uncertainty in the aerodynamic damping following the preceding equation based on the assigned uncertainties to various parameters was found to be equal to 0.3. The propagation of uncertainty resulted in a COV of 0.575 in the acrosswind bending moment. The structural and aerodynamic damping contributed COVs of 0.369 and 0.153, respectively.

7. Concluding remarks

Structural, aerodynamic and hydrodynamic damping mechanisms are each separately treated and recent advances in each summarized. The estimation of damping by the random decrement technique is presented in some detail. Examples show the utility of the method compared to spectral methods which are subject to resolution restrictions, and also show the limitations of the method in that its application requires nearly white noise input and a nearly linear system. The present state of the art in the design of tall buildings does not permit accurate damping estimates until the building construction is complete. In view of this uncertainty, the methodologies illustrated here offer a convenient tool for the estimation of building response with uncertain damping.

Acknowledgements

The support for this study was in part provided by ONR Grant No. 00014-93-1-0761 and NSF Grant Nos. CMS-9503779 and CMS-9402196. The second author was partially supported by a GAANNP fellowship. The authors thank Michael Tognarelli for his assistance in the preparation of this paper.

References

Basu, R.I. and B.J. Vickery (1983) Acrosswind vibrations of structures of circular cross section, Part II: development of a model for full-scale applications, J. Wind Eng. Ind. Aerodyn. 12, 75–97.

Boggs, D.W. (1992) Validation of the aerodynamic model method, J. Wind Eng. Ind. Aerodyn. 42, 1011–1022.

Braun, S. and A. Sneor, On the accuracy of parametric and classical spectra, J. Vibration. Acoustic Stress Reliability in Design, ASME 110, 213–219.

Breukelman, B., A. Dalgleish and N. Isyumov (1993) Estimates of damping and stiffness for tall buildings, in: Proc. 7th U.S. National Conf. on Wind Engineering, June, UCLA, Los Angeles.

Celebi, M. and E. Safak (1991) Recorded seismic response of Transamerica building. Part I: data and preliminary analysis, J. Struct. Eng. ASCE.

Cole, H.A. (1973) On-line failure detection and damping measurement of aerospace structures by the random decrement signatures, NASA CR-2205.

Davenport, A.G. and Hill-Carroll (1986) Damping in tall buildings: its variability and treatment in design, ASCE Spring Convention, Seattle, USA, Building Motion in Wind, 42–57.

ESDU, 1983, Damping of structures, part I: tall buildings, Engineering Science Data Units, Item No. 83009, London.

Gurley, K. and A. Kareem (1993) Gust loading factors for tension leg platforms, Appl. Ocean Res. 15, 137–154.

Gurley, K. and A. Kareem (1995) On the analysis and simulation of random processes utilizing higher order spectra and wavelet transforms, in: Proc. Int. Conf. on Computational Stochastic Mechanics (A.A. Balkema Press, Netherlands).

Hart, G.C. and R. Vasudevan (1975) Earthquake design of buildings: damping, J. Struc. Div. ASCE, 101 (ST1), 49–65.

Haviland, R. (1976) A study of the uncertainties in the fundamental translational period and damping values for real buildings, MIT, Research Report No. 5, Pub. No. R76-12, Dept. of Civil Eng. Cambridge, MA.

Hudson, D. E. (1977) Dynamic tests of full-scale structures, J. Eng. Mech Div. ASCE 103 (EM6), 1141–1157.

James, H.M. et al. (1947), Theory of Servomechanisms, MIT Radiation Laboratory Series, Vol. 25 (McGraw-Hill, New York).

Jeary, A.P. (1986) Damping in tall buildings – a mechanism and a predictor, Earthquake Eng. Struct. Dyn. 14, 733–750.

Jeary, A.P. (1992) Establishing non-linear damping characteristics of structures from non-stationary response time-histories, Struct. Eng. 70 (4), 61–66.

Jeary, A.P. and B.R. Ellis (1981) Vibration tests of structures at varied amplitudes, in: Proc. ASCE/EMD Specialty Conf. on Dynamic Response of Structures, ASCE, Atlanta, GA.

Jones, N.P. and C.A. Spartz (1990) Structural damping estimates for long-span bridges, J. Eng. Mech. 116 (11), 2414–2433.

Kareem, A. (1978) Wind excited motion of buildings, Thesis presented to Colorado State University at Fort Collins, Colorado, in partial fulfilment of the requirements for the degree of Doctor of Philosophy.

Kareem, A. (1981a) Wind-excited response of buildings in higher modes, J. Struct. Eng. ASCE 107 (ST4) 701–706.

Kareem, A. (1981b) Discussion of wind-induced lock-in excitation of tall structures by K.C.S. Kwok and W.H. Melbourne, J. Struct. Eng. ASCE 107 (ST1), J. Struct. Eng. ASCE 107 (ST10).

Kareem, A. (1982) Acrosswind response of buildings, J. Struct. Div. ASCE 108 (ST4), April, 869–887.

Kareem, A. (1988) Aerodynamic response of structures with parametric uncertainties, Structural Safety 5, 205–255.

Kareem, A. and W.J. Sun (1989) Dynamic response of structures with uncertain damping, Eng. Struct. 12(1).

Kwok, K.C.S. and W.H. Melbourne (1981) Wind-induced lock-in excitation of tall structures, J. Struct. Div. ASCE 107 (ST1), 57–72.

Lagomarsino, S. (1993) Forecast models for damping and vibration periods of buildings, J. Wind Eng. Ind. Aerodyn. 50, 309–318.

Li, Y. and A. Kareem (1990a) Recursive modeling of dynamic systems, J. Eng. Mech., ASCE 116 (3).
Li, Y. and A. Kareem (1990b) ARMA systems in wind engineering, Probab. Eng. Mech. 5 (2).
Li, Y. and A. Kareem (1993) Parametric modelling of stochastic wave effects on offshore platforms, Appl. Ocean Res. 15 (2).
Nashif, A.D., D.G. Jone and J.P. Henderson (1984) Vibration Damping (Wiley, New York).
Novak, M. (1971) Data reduction from nonlinear response curves, J. Eng. Mech. Div., ASCE 97 (EMD), 1187–1204.
Novak, M. (1974) Effect of soil on structural response to wind and earthquake, Earthquake Eng. Struct. Dyn. 3.
O'Rourke, M.O. (1976) Discussion on response of stochastic wind of N-degree tall buildings ASCE Proceedings Paper 12112, J. Struct. Eng. ASCE 102 (ST12), 2401–2403.
Otsuki, Y., K. Washizu, H. Tomizawa and A. Ohya (1974) A note on the Aeroelastic instability of a prismatic bar with square section, J. Sound Vib. 34 (2), 233–248.
Raggett, J.D. (1975) Estimating damping of real structures, J. Struct. Div. ASCE 101 (ST9) 1823–1835.
Safak, E. (1989) Adaptive modelling, identification and control of dynamic structural systems, J. Eng. Mech. ASCE 115 (1).
Saunders, J.W. and W.H. Melbourne (1975) Tall rectangular building response to cross-wind excitation, in: Proc. 4th Int. Conf. on Wind Effects on Buildings and Structures, Cambridge University Press, Cambridge, 369–379.
Scanlan, R.H. and J.J. Tomko (1971) Airfoil and bridge deck flutter derivatives, J. Eng. Mech. (EM6), 1717–1737.
Steckley, A. (1989) Motion induced wind forces on chimneys and tall buildings, Ph.D. thesis, University of Western Ontario, London, Canada.
Tamura, Y., A. Sasaki, T. Sato and R. Kousaka (1992) Evaluation of damping ratios of buildings during gusty winds using the random decrement technique, in: Proc. 12th Wind Eng. Symp.
Tamura, Y., K. Shimada, A. Sasaki, R. Kohsaka and K. Fuji (1995) Variation of structural damping ratios and natural frequencies of tall buildings during strong winds, in: Proc. 9th Int. Conf. on Wind Eng. (Wiley Eastern, New Delhi).
Tamura, Y., M. Yamada and H. Yokota (1994) Estimation of structural damping of buildings, ASCE Struct. Cong. and IASS Int. Symp., Atlanta, USA, Vol. 2, 1012–1017.
Taoka, G.T., M. Hogan, F. Khan and R.H. Scanlan (1975) Ambient response analysis of some tall structures, J. Struct. Eng. 101 (ST1), 49–65.
Trifunac, M.D. (1972) Comparisons between ambient and forced vibration, Earthquake Eng. Struct. Dyn. 1, 133–150.
Vandiver, J.K., A.B. Dunwoody, R.B. Campbell and M.F. Cook (1982) A mathematical basis for the random decrement vibration signature analysis technique, J. Mech. Design 104, 307–331.
Watanabe, Y., N. Isyumov and A.G. Davenport (1995) Empirical aerodynamic damping function for tall buildings, in; Proc. 9th Int. Conf. on Wind Eng. (Wiley Eastern, New Delhi) 1362–1371.
Wolf, J.P. (1988) Soil-Structure-Interaction Analysis in Time Domain (Prentice Hall, Englewood Cliffs, NJ).
Yang, J.C.S., N.G. Dagalakis, G.C. Everstine and Y.F. Wang (1983) Measurement of structural damping using the random decrement technique, Shock Vibration Bull. 53 (4), 63–71.
Yokoo, Y. and H. Akiyama (1972) Lateral vibration and damping due to wind and earthquake effects, in: Proc. Int. Conf. on Planning and design of Tall Buildings, Vol. II-17, ASCE, NY.